Thermochimica Acta 651 (2017) 73–82

Contents lists available at ScienceDirect

Thermochimica Acta

journal homepage: www.elsevier.com/locate/tca

Thermal behavior, spectroscopic studies and free radical scavenging potential of some mefenamate trivalent lanthanides (Sm, Eu, Gd, Tb and Dy)

Francisco X. Campos[a,b], André L.C.S. Nascimento[a], Tiago A.D. Colman[a], Diogo A. Gálico[c], Ana C.S. Carvalho[d], Flávio J. Caires[e], Adriano B. Siqueira[d], Massao Ionashiro[a,*]

[a] Instituto de Química, UNESP – Campus Araraquara, CEP 14801-970 Araraquara, SP, Brazil
[b] Instituto Federal de Educação, Ciência e Tecnologia de Mato Grosso, IFMT – Campus Primavera do Leste, CEP 78850-000 Primavera do Leste, MT, Brazil
[c] Instituto de Química, UNICAMP – Universidade Estadual de Campinas, CEP 13083-970, Campinas, SP, Brazil
[d] Universidade Federal de Mato Grosso, UFMT – Campus Cuiabá, CEP 78060-900 Cuiabá, MT, Brazil
[e] Faculdade de Ciências, UNESP – Campus Bauru, CEP 17033-260 Bauru, SP, Brazil

ARTICLE INFO

Article history:
Received 29 November 2016
Received in revised form 25 February 2017
Accepted 5 March 2017
Available online 6 March 2017

Keywords:
Mefenamate
Lanthanides
Thermal analysis
EGA
Spectroscopy
DPPH

ABSTRACT

Lanthanide Mefenamate compounds were prepared in solid state. TG-DSC coupled to FTIR, elemental analysis, complexometry with EDTA, X-ray powder diffractometry, evaluation of scavenging free radical activity with DPPH (2,2-diphenyl-1-picryl-hydrazine), and a complete spectroscopic study in the ultraviolet, visible, near-, and middle-infrared regions were realized to obtain some physicochemical properties of the synthesized compounds. The thermal stability, minimum formula, thermal behavior and intermediate compounds were indicated by thermoanalytical results. Furthermore, vibrational spectroscopy data suggests that the complexes are binuclear and two modes of coordination are presented. The DR spectra could be reveal the presence of a large ligand-to-metal charge transfer band in the europium mefenamate. This compound also indicated the higher antioxidant activity with DPPH (77.03% at 200 $\mu g\,L^{-1}$).

1. Introduction

Rare earth elements have been studied in order to develop materials for technological applications, mainly because of their thermal behavior and their spectroscopic and magnetic properties [1–4].

Non-steroidal anti-inflammatory drugs (NSAID) were used as ligands to associate with d-block transition metals, which demonstrated other properties such as free radical scavenging ability [4,5].

Recently, the association of rare earth elements with NSAIDs has shown promising signs for new research. Examples include the finding that ketoprofen [6,7] and naproxen [8] compounds exhibit more anti-inflammatory activity than free ligands. Europium complexe of ketoprofen have an intriguing luminescent property and can be used as a nanothermometer due to its strong temperature dependence [9]. Terbium compounds produced by carproxen have also exhibited strong energy transfer between the ligand and the metal, which leads to a substantial luminescent property [10]. The f-block metals associated with NSAID are important because they exhibit different properties, including pharmacological activity (free radical scavenging ability) and technological characteristics (magnetism, conductivity, luminescence and electroluminescence) [2,11].

Mefenamic acid is classified as a NSAID due to its antiproliferative and antioxidant properties. These properties were found to be enhanced when coordinated with certain bivalent transition metals, and this enhancement makes the development of new drugs possible [4,5,12].

Antioxidant action is important for the restoration of homeostasis and for treating diseases originating from free radicals [3,13,14]. Some papers have demonstrated that the compounds exhibiting antioxidant activity could be used as anticancer drugs, or as anti-aging and anti-inflammatory agents [13–15]. The DPPH method is used extensively to evaluate antioxidant activity, and it has presented reliable results [16–19].

The compounds were investigated through the use of complexometry, elemental analysis, X-ray powder diffractometry, simultaneous thermogravimetry, and differential scanning calorimetry (TG-DSC), TG-DSC combined with infrared spectroscopy, a complete spectroscopic study in the ultraviolet, visible, near-, and

* Corresponding author.
E-mail address: massaoi@iq.unesp.br (M. Ionashiro).

http://dx.doi.org/10.1016/j.tca.2017.03.002
0040-6031/

Table 1
Analytical and thermoanalytical (TG) results for the $Ln(Mef)_3$ compounds.

Compounds	Ln (oxide)/%			Mef (lost)/%		C/%			H/%			N/%			Residue
	Calc.	TG	EDTA	Calc.	TG	Calc.	TG	EA	Calc.	TG	EA	Calc.	TG	EA	
$Sm(Mef)_3$	20.01	19.88	20.23	79.99	80.12	62.03	62.13	61.69	5.10	5.11	4.80	4.82	4.83	4.50	Sm_2O_3
$Eu(Mef)_3$	20.16	20.43	20.02	79.84	79.57	61.91	61.70	62.27	5.09	5.07	4.83	4.81	4.79	5.12	Eu_2O_3
$Gd(Mef)_3$	20.64	20.44	20.21	79.36	79.56	61.54	61.70	61.94	5.06	5.07	4.45	4.79	4.80	5.04	Gd_2O_3
$Tb(Mef)_3$	21.25	21.07	21.20	78.75	78.93	61.43	61.57	61.15	5.05	5.06	5.12	4.78	4.79	4.49	Tb_4O_7
$Dy(Mef)_3$	21.11	21.39	21.25	78.89	78.61	61.18	60.96	60.75	5.03	5.01	5.20	4.79	4.74	4.40	Dy_2O_3

Ln = Lanthanides; Mef = mefenamate.

middle-infrared regions, and evaluation of free radical scavenging activity using DPPH (2,2-diphenyl-1-picryl- hydrazine).

2. Materials and methods

Mefenamic acid ($C_{15}H_{15}NO_2$/99.6%), H-Mef, was obtained from Sigma-Aldrich, and it was used as received. The purity of H-Mef was determined by DSC [4]. The lanthanides were prepared from the metal oxides sigma c.a. 99.9% (Sm_2O_3, Eu_2O_3, Gd_2O_3, Tb_4O_7 and Dy_2O_3).

The lanthanide (Sm to Dy) mefenamates were prepared following the same procedure described in the literature [11].

In the solid-state, metal ions, hydration water and mefenamate contents were determined from TG curves. The metal ions were also determined by complexometry using standard EDTA solution, after igniting the compounds to the respective oxides and their dissolution in hydrochloric acid solutions [20].

Carbon, hydrogen and nitrogen contents were determined by microanalytical procedures, with CHN elemental analyzer from Perkin Elmer, model 2400, and from TG curves.

Simultaneous thermogravimetry and differential scanning calorimetry curves (TG-DSC) were obtained using a thermogravimetric analyzer system from Mettler-Toledo. Air or N_2 were used as purge gas with flow of 50 mL min^{-1}. A heating rate of 10 °C min^{-1} was adopted, with samples weighing c.a. 5 mg using Alumina crucibles. The evolved gas analysis (EGA) was performed using TG-DSC thermogravimetric analyzer coupled to FTIR Nicolet spectrophotometer with gas cell and DTGS KBr detector. The furnace and heated gas cell (250 °C) were coupled through a heated (225 °C) 120 cm stainless steel line transfer with diameter of 3.0 mm, both purged with 50 mL min^{-1}. The FTIR spectra were recorded with 16 scans per spectrum at a resolution of 4 cm^{-1}.

X-ray powder patterns were obtained by using a Bruker AXS D8 Advance X-ray diffractometer employing CuKa radiation (k = 1.544 Å) and setting of 40 kV and 40 mA.

Diffuse reflectance (DR) spectra were acquired using a Varian Cary 5000 spectrophotometer within the 270–1000 nm range with spectral resolution of 0.5 nm.

Near-infrared spectra (NIR) were collected using a Thermo Scientific Antaris II spectrophotometer by reflectance, within the 1000–2500 nm range.

Middle infrared spectra (MIR) were run on a Nicolet iS10 Fourier transform infrared spectrophotometer (FTIR), using an ATR accessory with Ge window. The MIR spectra were recorded in the region of 4000–600 cm^{-1} with 32 scans per spectrum at the resolution of 4 cm^{-1}.

Raman spectra were obtained on a Horiba Jobin-Yvon T64000 using a He/Ne laser (λ = 632.8 nm) and a spectral resolution of 2 cm^{-1}. The spectra were acquired in the 1700–1300 cm^{-1} range.

The evaluation of scavenging free radical activity with DPPH (2,2-diphenyl-1-picryl-hydrazine) were performed to H-Mef and synthesized compounds. The compounds were solubilized in methanol to obtain a stock solution from 20,0 mg L^{-1}. The stock solutions were diluted to 200 μgL^{-1}, 150 μgL^{-1}, 100 μgL^{-1}, 50 μgL^{-1}.

The solution to be analyzed were continuous stirring at room temperature by 30 min after mixing of 1.00 mL of DPPH methanolic solution 0,100 mmol L^{-1} and 3.00 mL of each diluted solution.

The resulting solutions were used in UV–vis spectrophotometer (Varian Cary 50 scan), the absorbance was recorded at 515 nm [16–18]. The determination of evaluation of scavenging free radical activity (AA) was performed with follow Eq. (1):

$$AA\,(\%) = 100 - \frac{\left(Abs_{(sample)} - Abs_{(blank)}\right).100}{Abs_{(control)}} \quad (1)$$

where $Abs_{(sample)}$ is the absorbance of the solution of synthesized compounds and DPPH, $Abs_{(blank)}$ is the absorbance of methanol, and $Abs_{(control)}$ is the absorbance of the solution of methanol and DPPH [19].

3. Results and discussion

3.1. Thermal analysis

The analytical and thermoanalytical (TG) data on the synthesized compounds is shown in Table 1. These results allowed us to establish the stoichiometry of these compounds, which is in agreement with the general formula $Ln(Mef)_3$, where Ln represents trivalent lanthanides (Sm to Dy) and Mef is mefenamate. The thermoanalytical results showed that the compounds were obtained in their anhydrous state.

These curves also show that the thermal stability (I) and the final temperature of the thermal decomposition (II) of these compounds depend on the nature of the metal ions and the purge gas (see Fig. 1 and Table 2), and they follow this order:

I) (air) Sm > Tb > Dy > Eu > Gd/(**N_2**) Tb > Sm = Dy > Eu > Gd
II) (air) Tb > Gd > Dy > Sm > Eu/(**N_2**) Dy > Tb > Sm = Gd > Eu

Because the TG-DSC profiles are characteristic of each atmosphere, they are presented based on this characteristic.

3.1.1. TG-DSC in the air atmosphere

The TG-DSC curves in dynamic dry air atmospheres are shown in Fig. 1(a–e). These curves show that the mass losses occur in three consecutive and overlapping steps with thermal events corresponding to these losses. Substantial similarity is noted among the TG-DSC profiles of these compounds.

These curves also show that the first two mass losses occur through a fast process that corresponds to exothermic peaks, which themselves are attributed to oxidation of the organic matter and/or of the gaseous products that evolve during the thermal decomposition, with the formation of carbonaceous residue and/or a derivative of carbonate. Tests using a hydrochloric acid solution on samples heated up to the temperatures at which these intermediates form (as indicated by the corresponding TG-DSC curves),

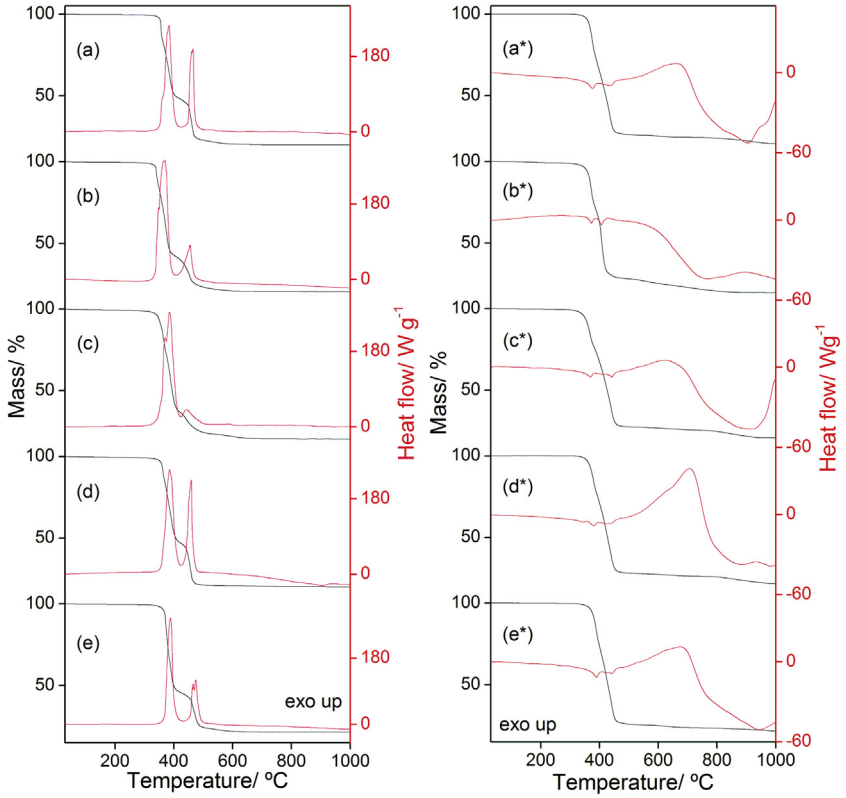

Fig. 1. TG–DSC curves of the compounds in dynamic air atmospheres (left): (a) $Sm(Mef)_3$ (5.100 mg), (b) $Eu(Mef)_3$ (5.238 mg), (c) $Gd(Mef)_3$ (5.040 mg), (d) $Tb(Mef)_3$ (5.082 mg), (e) $Dy(Mef)_3$ (5.030 mg); TG–DSC curves in N2* atmospheres (right): (a*) $Sm(Mef)_3$(5.077 mg), (b*) $Eu(Mef)_3$ (5.012 mg), (c*) $Gd(Mef)_3$ (5.067 mg), (d*) $Tb(Mef)_3$ (5.007 mg), (e*) $Tb(Mef)_3$ (5.091 mg).

Table 2
Temperatures ranges (θ), mass losses (Δm) and peak temperatures (T_P) observed for each step of the TG-DSC curves of the $Ln(Mef)_3$ compounds.

Compounds	Steps							Total Δm	
		first		second		third			
		air	N_2	air	N_2	air	N_2	air	N_2
$Sm(Mef)_3$	θ/°C	320–405	315–380	405–480	380–460	480–620	460–955	80.12	79.28
	Δm/%	50.42	22.04	25.98	50.81	3.72	6.43		
	T_P/°C	380 ↑	380 ↓	460 ↑	440 ↓	535 ↓	905 ↓		
$Eu(Mef)_3$	θ/°C	290–390	300–380	390–470	380–455	470–610	455–860	79.57	80.33
	Δm/%	56.53	27.10	18.43	43.90	4.51	9.33		
	T_P/°C	360 ↑	370 ↓	450 ↑	405 ↓	–	760 ↓		
$Gd(Mef)_3$	θ/°C	280–410	295–370	410–500	370–470	500–660	470–955	79.56	79.23
	Δm/%	62.67	19.86	12.90	52.06	3.99	7.31		
	T_P/°C	375↑	370 ↓	440 ↑	440 ↓	585 ↑	915 ↓		
$Tb(Mef)_3$	θ/°C	310–415	320–390	415–485	390–460	485–700	460–975	78.93	78.28
	Δm/%	51.50	21.65	26.21	49.27	1.22	7.36		
	T_P/°C	370 ↑	380 ↓	460 ↑	440 ↓	–	880 ↓		
$Dy(Mef)_3$	θ/°C	305–410	315–397	410–500	397–465	500–640	465–980	78.61	78.51
	Δm/%	53.11	22.84	22.76	50.35	2.74	5.32		
	T_P/°C	380 ↑	390 ↓	465, 470 ↑	440 ↓	535 ↑	945 ↓		

sm = small; ↑ exo; ↓ endo; Mef = mefenamate.

confirmed the evolution of CO_2 and the presence of the carbonaceous residue in all cases, with the exception of terbium, for which only carbonaceous residue was observed [11].

The last step is slow and the TG curves exhibited different mass losses, depending on the amount of carbonate derivative and carbonized material formed in the previous steps and no thermal event associated with this mass loss is observed on the DSC curve, probably because endothermic events (carbonate derivative decomposition) and exothermic event (oxidation of carbonized waste) occur simultaneously. The final residues obtained were their respective metal oxides, Tb_4O_7, and Ln_2O_3 (Ln = Sm, Eu, Gd, Dy), as shown in Table 2.

3.1.2. TG-DSC in the nitrogen atmosphere

The TG-DSC curves in the dynamic dry nitrogen atmosphere are shown in Fig. 1(a*–e*). The respective $Ln(Mef)_3$ compounds exhibited higher thermal stability in the nitrogen atmosphere, see Table 2, this phenomenon can be explained by presence of O_2 in

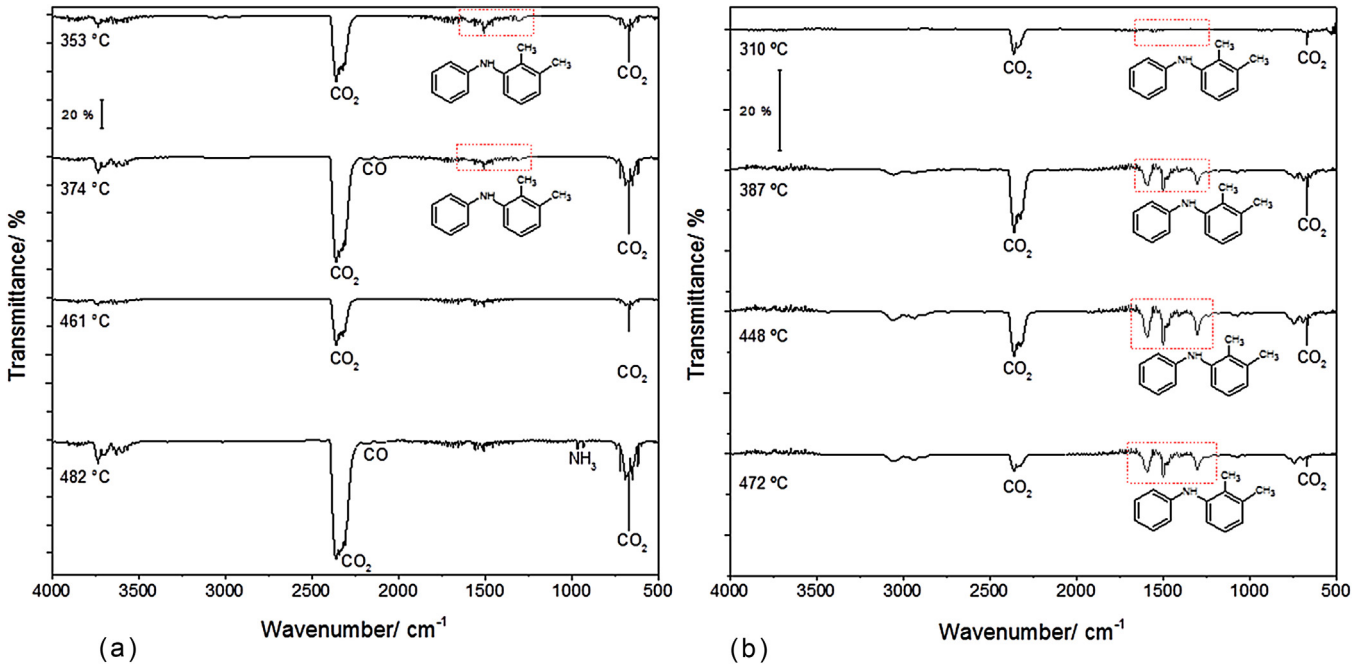

Fig. 2. IR spectra of gaseous products evolved during the thermal decomposition of the $Sm(Mef)_3$ in air atmosphere (a) and in N_2 atmosphere (b), as representative of all the compounds.

the air, which provokes an oxidation reaction and decreases the thermal stability in the air atmosphere.

These curves show that thermal decomposition occurs in three steps of mass loss, associated with endothermic events in the DSC curves. The profiles of the thermoanalytical curves of the compounds are very similar, a result which suggests the same thermal decomposition mechanism. The first two mass losses are a fast process and correspond to endothermic peaks at 380 °C and 440 °C (Sm), 370 °C and 405 °C (Eu), 370 °C and 440 °C (Gd), 380 °C and 440 °C (Tb), and 390 °C and 440 °C (Dy). These values are attributed to thermal decomposition with the formation of carbonaceous residue.

The last mass loss step also occurs slowly and corresponds to endothermic peaks at 905 °C (Sm), 760 °C (Eu), 915 °C (Gd), 880 °C (Tb), and 945 °C (Dy). These step is attributed to the pyrolysis of the carbonaceous residue with the formation of the respective oxides Tb_4O_7 and Ln_2O_3 (Ln = Sm, Eu, Gd, Dy).

Part of the residue formed of decomposition of the $Tb(Mef)_3$ is reduced from Tb_4O_7 to Tb_2O_3 in 905 °C, evidenced for an endothermic event and small mass loss

(0,4%), this phenomenon occur due oxygen deficiency and high temperature.

The temperature ranges (θ), mass losses (Δm) and peak temperatures (Tp) observed for each step of the TG-DSC curves also are shown in Table 2.

3.1.3. Evolved gas analysis (EGA)

The infrared spectra of gaseous products were selected at different temperatures during the thermal decomposition of $Sm(Mef)_3$ (see Fig. 2) as representative of all of the compounds.

Analysis of the spectra shows that the main gaseous products released in air atmosphere were CO_2, CO, 2,3-dimethyl-*N*-phenylaniline and NH_3 [11]. Already in nitrogen atmosphere only CO_2 and 2,3-dimethyl-N-phenylaniline were identified. These results suggest that the thermal decomposition occurs mainly via decarboxylation and the oxidizing atmosphere has a pronounced influence on the thermal behavior.

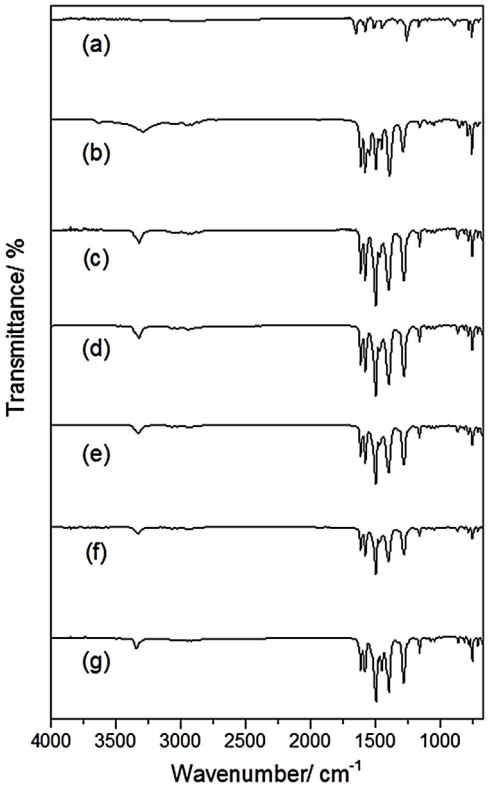

Fig. 3. MIR spectra of (a) Mefenamic acid, (b) sodium salt, (c) $Sm(Mef)_3$, (d) $Eu(Mef)_3$, (e) $Gd(Mef)_3$, (f) $Tb(Mef)_3$ and (g) $Dy(Mef)_3$.

3.2. Vibrational spectroscopy

Fundamental vibrational transitions were studied in terms of both MIR and Raman spectroscopy due to the differences in the two method's selection rules. As a consequence, some transitions

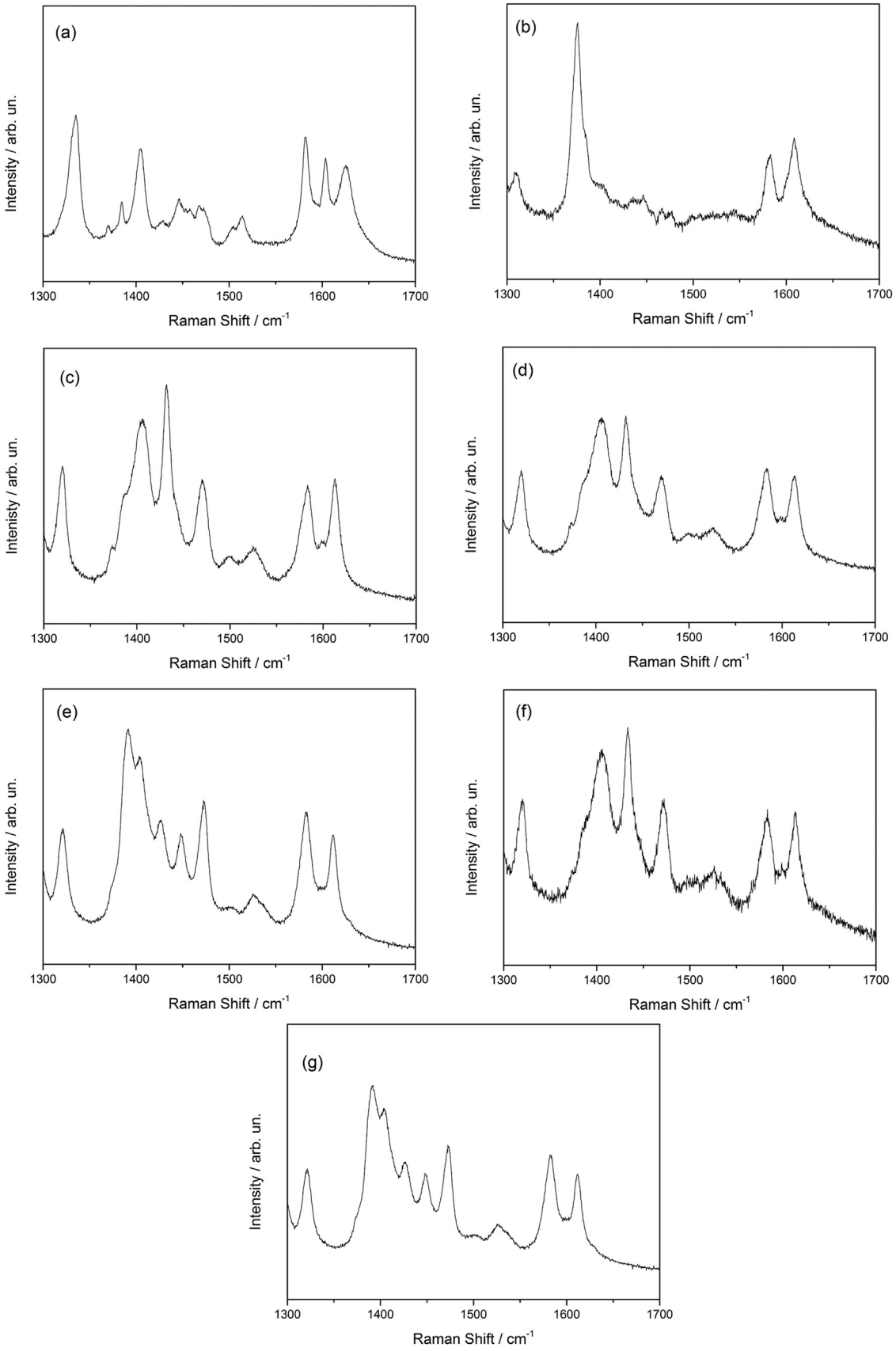

Fig. 4. Raman spectra of (a) Mefenamic acid, (b) sodium salt, (c) $Sm(Mef)_3$, (d) $Eu(Mef)_3$, (e) $Gd(Mef)_3$, (f) $Tb(Mef)_3$, (g) $Dy(Mef)_3$.

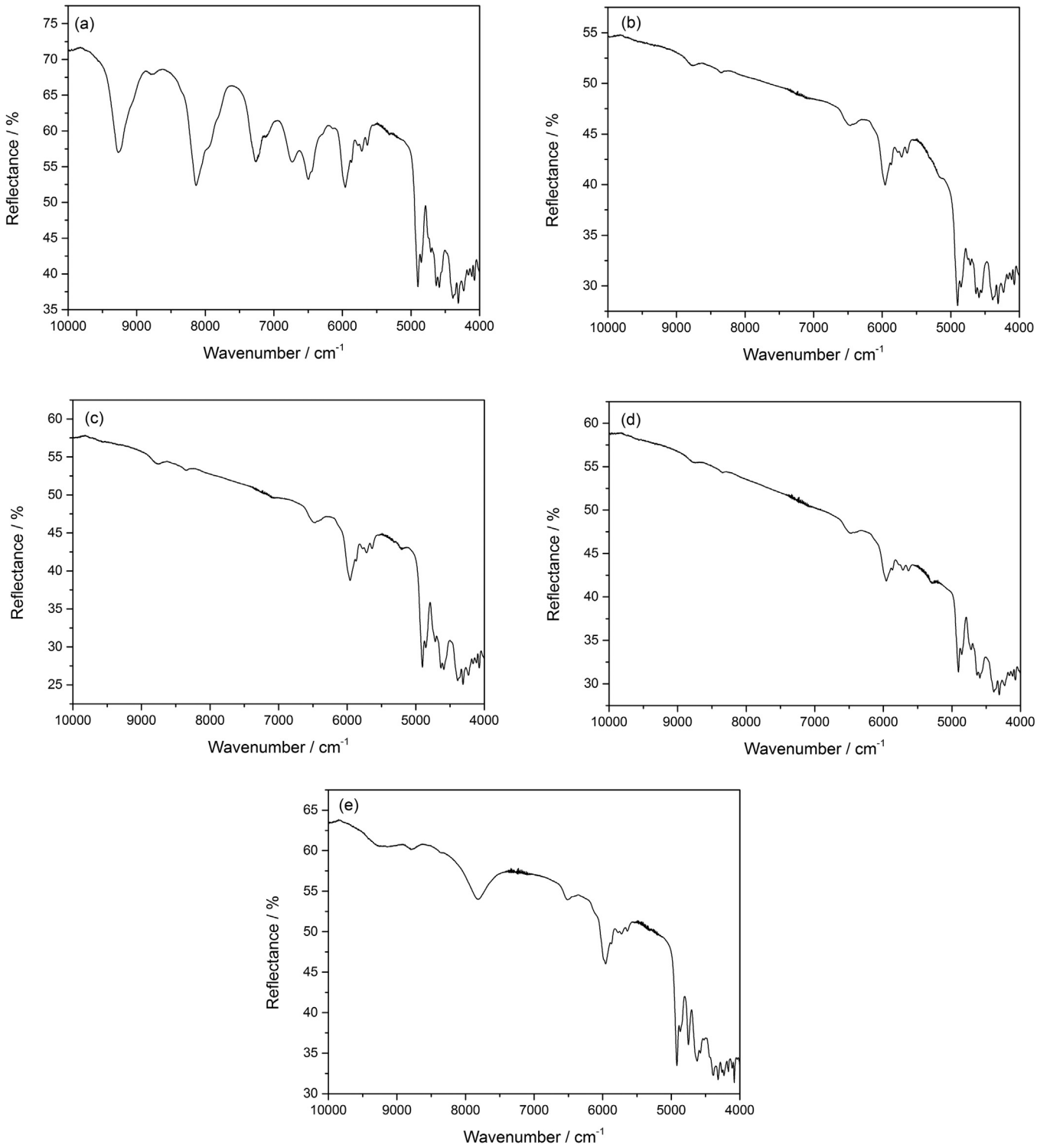

Fig. 5. NIR spectra of (a) $Sm(Mef)_3$, (b) $Eu(Mef)_3$, (c) $Gd(Mef)_3$, (d) $Tb(Mef)_3$ and (e) $Dy(Mef)_3$.

that are forbidden in infrared spectroscopy are permitted in Raman spectroscopy.

The MIR spectra of the H-Mef, Na-Mef, and lanthanide mefenamates are shown in Fig. 3, and some frequencies of the mefenamic compounds along with their assignments are presented in supplementary material (Table S1). The Raman spectra of the compounds are shown in Fig. 4, and some assignments are presented in supplementary material (Table S2). The main vibrational modes of H-Mef are associated with carbon-oxygen stretching frequencies of the carboxylic group (νC=O) and nitrogen-hydrogen stretching (νN–H), carbon-nitrogen stretching (νC–N), nitrogen-hydrogen deformation in plane (δN–H) [20], and nitrogen-hydrogen rocking vibrations [21] of the amine group. The bands at 1649 cm^{-1} and 1626 cm^{-1} of the MIR and Raman spectra, respectively, were due to the νC=O stretching of the carboxylic acid of

H-Mef. These bands were not observed in the case of the $Ln(Mef)_3$ spectra. The absence of this band on the salt and complex spectra confirms that they do not contain any acid contamination.

Table 3
Antioxidant activity (%) with DPPH of mefenamic acid and $Ln(Mef)_3$ compounds after 30 min.

Compounds	Concentration in methanol of compounds/$\mu g\,L^{-1}$			
	50	100	150	200
HMef	25.80 (±0.09)	26.11 (±0.32)	29.40 (±0.13)	37.85 (±1.02)
$Sm(Mef)_3$	27.75 (±0.73)	27.98 (±0.57)	29.69 (±0.26)	30.64 (±0.24)
$Eu(Mef)_3$	31.41 (±0.03)	56.28 (±0.59)	58.15 (±0.05)	77.03 (±0.09)
$Gd(Mef)_3$	28.69 (±0.05)	31.08 (±0.23)	34.11 (±0.07)	38.67 (±0.10)
$Tb(Mef)_3$	21.79 (±0.30)	30.58 (±0.06)	31.37 (±0.14)	38.11 (±0.17)
$Dy(Mef)_3$	29.39 (±0.19)	32.43 (±0.09)	32.25 (±0.05)	33.59 (±0.07)

HMef = mefenamic acid; Mef = mefenamate.

The characteristic bands of the C—N and N—H groups presented no significant shifts when compared to the acid, salt and the complexes, a finding which indicates that this group is not involved in coordination [22].

Carboxylate asymmetric stretching, or νas (COO^-), is centered at c.a 1610 cm^{-1} in the case of the sodium salt and the complexes. Carboxylate symmetric stretching, or νs (COO^-), is centered in the 1390 cm^{-1} region within the MIR spectra. The sodium salt was found to have only one band in this region, but in the case of the complexes, a shoulder is seen in the highest energy side of the band. The analysis of the Raman spectra revealed that the νs (COO^-) band of the complexes has two components, the less energetic of which is in the same region of the band in the sodium salt (c.a. 1390 cm^{-1}), and the most energetic of which was found at 1430 cm^{-1}. This result is an indicator of two possible coordination modes.

The values obtained as the difference between the carboxylate stretches, or $\Delta\nu = \nu as(COO^-) - \nu s(COO^-)$, were used as criteria to understand the metal-ligand interactions. Two values were found for $\Delta\nu$ for the complexes: the first is very close of the value obtained for the sodium salt (indicating an interaction involving bidentate bridging), while the second is smaller when compared to that of the salt (indicating a chelate interaction) [22,23].

The near-infrared region spectra of the $Ln(Mef)_3$ provided information on the combination and overtone bands of the compounds (see Fig. 5). The assignments and discussion of the H-Mef and the Na-Mef bands are consistent with literature [11]. The $Gd(Mef)_3$ assignment was found to be representative (see Table S3). In the cases of the other compounds, the band assignments were the same as that of gadolinium. The exceptions were only the samarium, europium, and dysprosium compounds, which exhibited bands that were assigned to *f-f* transitions. The absence of water bands in the compound spectra confirms that they are anhydrous, as observed by TG-DSC curves.

The data obtained from vibrational spectroscopy suggests that the compounds are binuclear, and two modes of coordination are presented, see Fig. 6. These similarities were indicated in TG-DSC discussion.

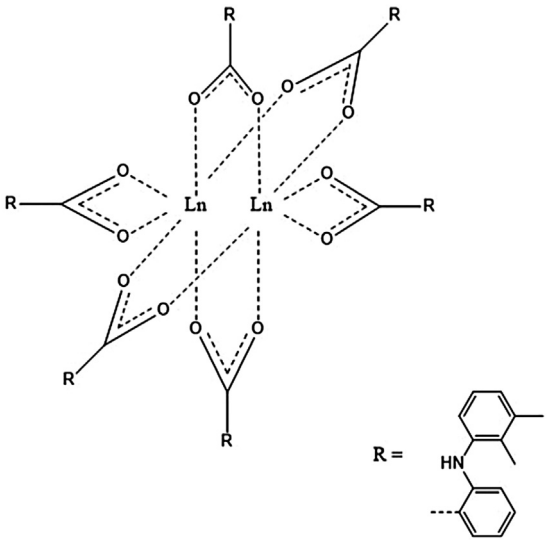

Fig. 6. Modes of coordination of the compounds from vibrational spectroscopy.

3.3. Electronic spectroscopy

Electronic transitions of the compounds were studied in the ultraviolet, visible, and near-infrared regions.

The diffuse reflectance (DR) spectra (200–1000 nm) of the Ln^{3+} compounds (Ln = Sm, Eu, Gd, Tb and Dy) are shown in Fig. 7. They exhibited a broad intra-ligand (IL) band in the UV and visible regions (270–460 nm). The exception was $Eu(Mef)_3$, for which this band was found to reach approximately 670 nm. This finding explains why all of the compounds exhibited a pale yellow color with the exception of $Eu(Mef)_3$, which exhibited a darker yellow color. The high intensity of this band masks the presence of the *4f-4f* transitions of the Ln^{3+} ions. The *4f-4f* transitions of the europium and terbium ions could not be seen and, in the case of the samarium and dysprosium, only a few transitions were seen.

The $Sm(Mef)_3$ spectra was found to exhibit two peaks that corresponded to the transitions from the 6H5/2 ground state to the excited states. The peaks at 476 nm and 945 nm are assigned to 4I11/2 ⟵ 6H5/2 and 6F11/2 ⟵ 6H5/2, respectively. The $Dy(Mef)_3$ spectra exhibited three peaks that corresponded to the transitions from the 6H15/2 ground state to the excited states. The peaks at 747 nm, 802 nm, and 894 nm are assigned to 6F3/2 ⟵ 6H15/2, 6F5/2 ⟵ 6H15/2, and 6F7/2 ⟵ 6H15/2, respectively.

In the NIR spectra (Fig. 5), $Sm(Mef)_3$, $Eu(Mef)_3$, and $Dy(Mef)_3$ exhibited characteristics *4f-4f* transitions. The $Sm(Mef)_3$ NIR spectra exhibited peaks located at 9268 cm^{-1}, 8134 cm^{-1}, 7264 cm^{-1}, 6734 cm^{-1}, 6503 cm^{-1}, and 5959 cm^{-1} (1079 nm, 1229 nm, 1377 nm, 1485 nm, 1538 nm, and 1678 nm), which were assigned to the 6F9/2 ⟵ 6H5/2, 6F7/2 ⟵ 6H5/2, 6F5/2 ⟵ 6H5/2, 6H3/2 ⟵ 6H5/2, 6F11/2 ⟵ 6H5/2,and 6F1/2 ⟵ 6H5/2 transitions, respectively. The 6H3/2 ⟵ 6H5/2 transition is hypersensitive. The $Eu(Mef)_3$ NIR spectra were found to exhibit a peak located at 5139 cm^{-1} (1946 nm), which was assigned to the 7F6 ⟵ 7F0 transition. $Dy(Mef)_3$ NIR spectra were found to have peaks located at 9285 cm^{-1} and 7822 cm^{-1} (1077 nm and 1278 nm), which were assigned to the 6F9/2 + 6H7/2 ⟵ 6H15/2 and 6F11/2 + 6H9/2 ⟵ 6H15/2 transitions, respectively. The 6F11/2 ⟵ 6H15/2 transition is hypersensitive.

To study the nature of the europium transition in the ultraviolet and visible regions, the arithmetic difference between the diffuse reflectance spectra in the solid states of the europium(III) and gadolinium(III) compounds was calculated, as shown in Fig. 8 [24]. The arithmetic difference revealed the presence of a very large ligand-to-metal ($O2- \rightarrow Eu3+$) charge transfer (LMCT) in the range 400–625 nm (25000–16000 cm^{-1}), in high resonance with the 5D1 and 5D0 emitter states of the europium ion, which can act as a

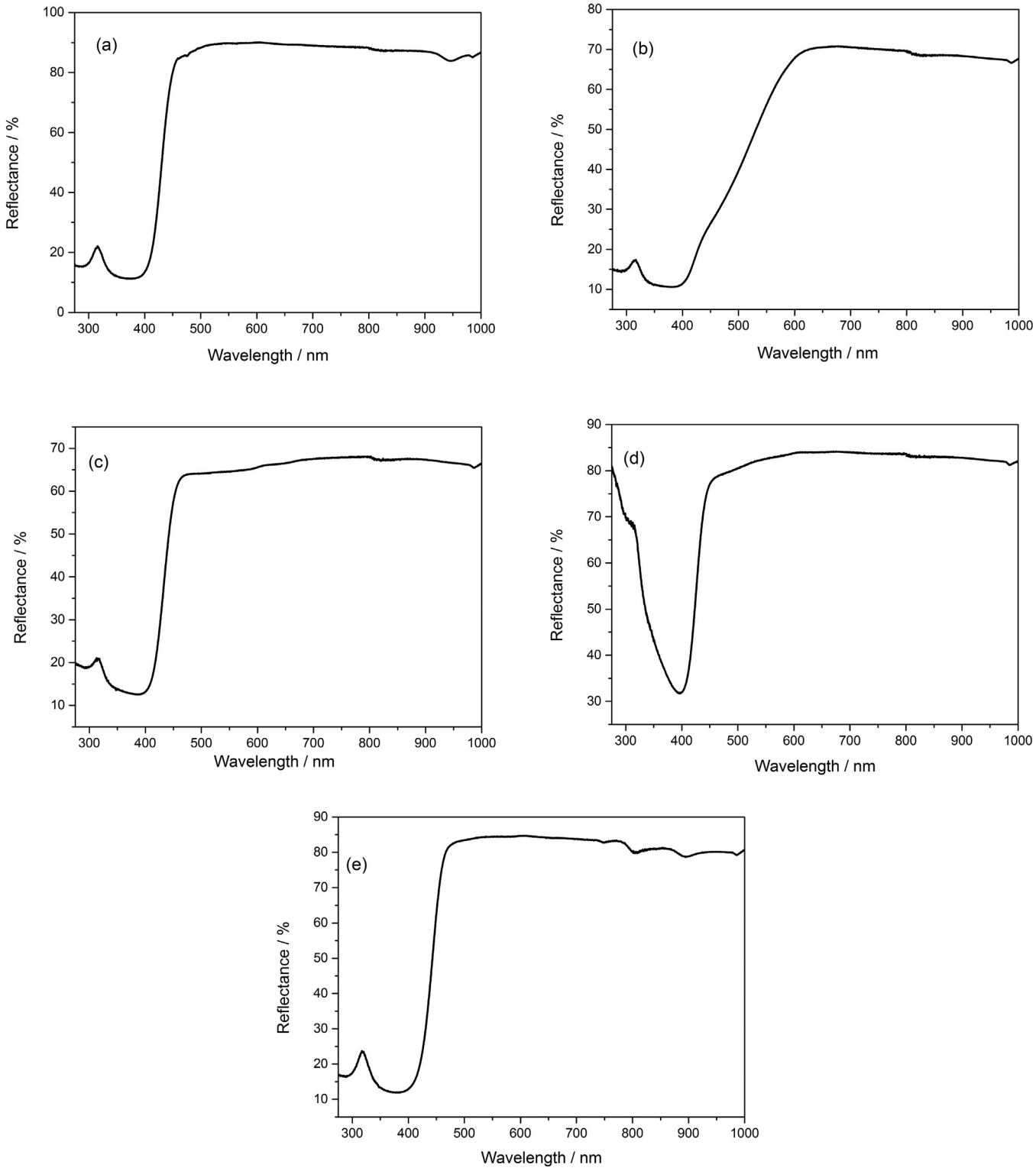

Fig. 7. DR spectra of (a) $Sm(Mef)_3$, (b) $Eu(Mef)_3$, (c) $Gd(Mef)_3$, (d) $Tb(Mef)_3$, (e) $Dy(Mef)_3$.

highly efficient quenching route in the energy transfer between the ligand and the europium ion [25].

3.4. XRD

The X-ray powder patterns showed that all of the compounds were obtained at a low crystallinity state (see Fig. S1).

3.5. Antioxidant Activity Evaluation (DPPH)

The evaluation of free radical scavenging activity with DPPH is presented in Table 3. All synthesized compounds exhibited higher activity than H-Mef at the concentrations analyzed, with the exception of the compounds from $Tb(Mef)_3$ at 50 $\mu g\,L^{-1}$, and $Sm(Mef)_3$

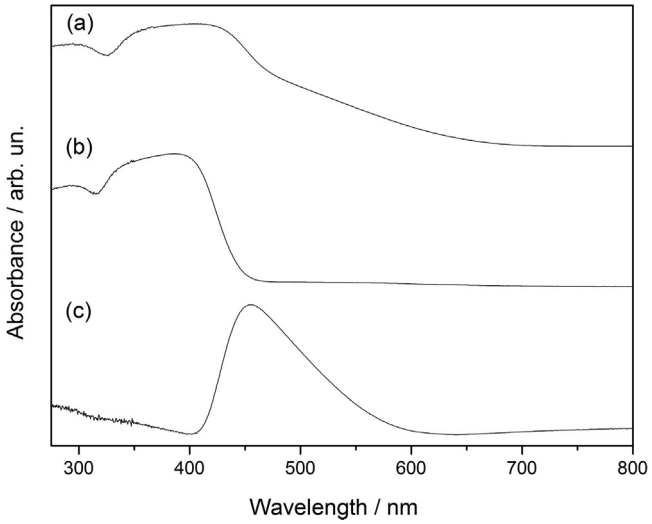

Fig. 8. DR spectra (in absorbance) of (a) $Eu(Mef)_3$, (b) $Gd(Mef)_3$ and (c) arithmetic difference between the europium(III) and gadolinium(III) compounds diffuse reflectance spectra showing the LMCT band.

and $Dy(Mef)_3$ at 200 $\mu g\,L^{-1}$. The $Eu(Mef)_3$ exhibted higher antioxidant capacity, with maximum values at 77.03% using 200 $\mu g\,L^{-1}$.

3.6. Qualitative solubility test

Qualitative tests provided information on approximate solubility at room temperature [26]. The results indicated that all of the compounds synthesized were practically insoluble (more than 10,000 mL per 1 g of solute) in water, ethanol, methanol and ether, and that they were freely soluble (1–10 mL per 1 g of solute) in dimethyl sulfoxide and dimethylformamide.

4. Conclusion

The data from the thermal analysis, complexometry, elemental analysis, and spectroscopy studies showed that all of the compounds are anhydrous with stoichiometry of the general formula $Ln(Mef)_3$, where Ln are trivalent lanthanides (Sm to Dy) and Mef is mefenamate. The data obtained from the vibrational spectroscopy suggests that the complexes are binuclear, and two modes of coordination are presented. The thermal analysis data provided previously unreported information on thermal stability, as well as on the thermal decomposition of these compounds in dynamic air and nitrogen atmospheres.

The EGA in nitrogen atmosphere suggest that the main mechanism of thermal decomposition is via decarboxylation with formation of diphenylamine and CO_2. On the other hand, in air atmosphere the main gaseous products released were CO_2, CO, 2,3-dimethyl-*N*-phenylaniline and NH_3, suggesting that the oxidizing atmosphere has a pronounced effect on the thermal behavior and consequently on the thermal decomposition mechanism.

The mid-infrared region spectroscopic data suggests that metal coordination to the carboxylate group is carried out and bidentate chelate form the metal is coordinated exclusively by the ligand by carboxylate group and that the coordination of metal with the carboxylate group is carried out and bidentate chelate mode, a finding which is corroborated by the near-infrared region data. Furthermore, the NIR spectra revealed *f-f* transitions bands in the samarium, europium, and dysprosium compounds.

The high absorption of the ligand in the ultraviolet and visible region overlaps most of the *f-f* transitions bands expected for this region. The arithmetic subtraction of the diffuse reflectance spectra from $Eu(Mef)_3$ and $Gd(Mef)_3$ revealed the presence of a large ligand-to-metal charge transfer band in $Eu(Mef)_3$.

The data from the evaluation of free radical scavenging activity suggests that the synthesized compounds exhibit higher activity antioxidant activity than H-Mef. The Europium compound showed higher antioxidant capacity, with a maximum value at 77.03% using 200 $\mu g\,L^{-1}$.

Acknowledgements

The authors thank FAPESP, CNPq and CAPES Foundations (Brazil) for financial support, and the Laboratório de Caracterização de Novos Materiais (LACANM/UFMT) – where of X-ray powder patterns were made. This research was supported by resources supplied by the Instituto de Quimica de Araraquara, UNESP Campus de Araraquara and CENAPAD-UNICAMP.

Appendix A. Supplementary data

Supplementary data associated with this article can be found, in the online version, at http://dx.doi.org/10.1016/j.tca.2017.03.002.

References

[1] M. Bottrill, L. Kwok, N.J. Long, Lanthanides in magnetic resonance imaging, Chem. Soc. Rev. 35 (2006) 557–571, http://dx.doi.org/10.1039/b516376p.
[2] J. Kido, Y. Okamoto, Organolanthanide metal complexes for electroluminescent materials, Chem. Rev. 102 (2002) 2357–2368, http://dx.doi.org/10.1021/cr010448y.
[3] M. Valcheva-Traykova, L. Saso, I. Kostova, Involvement of lanthanides in the free radicals homeostasis, Curr. Top. Med. Chem. 14 (2014) 2508–2519, http://dx.doi.org/10.2174/1568026614666141203123620.
[4] F.X. Campos, M.R.S. Soares, A.J. Terezo, A.B. Siqueira, Synthesis, characterization, and antioxidant evaluation of solid-state mefenamates of some bivalent metals, J. Therm. Anal. Calorim. 115 (2014) 167–176, http://dx.doi.org/10.1007/s10973-013-3275-0.
[5] J.J. Lozano, R. Pouplana, M. López, J. Ruiz, Conformational analysis of the antiinflammatory fenamates: a molecular mechanics and semiempirical molecular orbital study, J. Mol. Struct. Theochem. 335 (1995) 215–227, http://dx.doi.org/10.1016/0166-1280(94)04003-B.
[6] D.A. Gálico, B.B. Holanda, G.L. Perpétuo, E. Schnitzler, O. Treu-Filho, G. Bannach, Thermal and spectroscopic studies on solid Ketoprofen of lighter trivalent lanthanides, J. Therm. Anal. Calorim. 108 (2012) 371–379, http://dx.doi.org/10.1007/s10973-011-1866-1.
[7] D.A. Gálico, M.G. Lahoud, M.R. Davolos, R.C.G. Frem, T.F.C. Fraga-Silva, J. Venturini, M.S.P. Arruda, G. Bannach, Spectroscopic, luminescence and in vitro biological studies of solid ketoprofen of heavier trivalent lanthanides and yttrium(III), J. Inorg. Biochem. 140 (2014) 160–166, http://dx.doi.org/10.1016/j.jinorgbio.2014.07.008.
[8] Z.N. Chen, R.W. Deng, J.G. Wu, Synthesis, characterization, and antiinflammatory activity of Naproxen complexes with rare earth (III), J. Inorg. Biochem. 47 (1992) 81–87, http://dx.doi.org/10.1016/0162-0134(92)84044-N.
[9] M.G. Lahoud, R.C.G. Frem, D.A. Gálico, G. Bannach, M.M. Nolasco, R.A.S. Ferreira, L.D. Carlos, Intriguing light-emission features of ketoprofen-based Eu(III) adduct due to a strong electron-phonon coupling, J. Lumin. 170 (2015) 357–363, http://dx.doi.org/10.1016/j.jlumin.2015.08.050.
[10] X. Zhou, X. Zhao, Y. Wang, B. Wu, J. Shen, L. Li, Q. Li, Eu (III) and Tb (III) complexes with the nonsteroidal anti- in fl ammatory drug carprofen: synthesis, Cryst. Struct. Photophys. Prop. 3 (2014).
[11] F.X. Campos, Nascimento A.L.C.S, T.A.D. Colman, D.A. Gálico, O. Treu-Filho, F.J. Caires, A.B. Siqueira, M. Ionashiro, Synthesis, characterization and thermal behavior of solid state of some mefenamate of trivalent lanthanides (La, Ce, Pr and Nd), J. Therm. Anal. Calorim. 123 (2016) 91–103, http://dx.doi.org/10.1007/s10973-015-4956-7.
[12] D. Kovala-Demertzi, M. Staninska, I. Garcia-Santos, A. Castineiras, M.A. Demertzis, Synthesis, crystal structures and spectroscopy of meclofenamic acid and its metal complexes with manganese(II), copper(II), zinc(II) and cadmium(II). Antiproliferative and superoxide dismutase activity, J. Inorg. Biochem. 105 (2011) 1187–1195, http://dx.doi.org/10.1016/j.jinorgbio.2011.05.025.
[13] S.N. Misra, M.A. Gagnani, I.D. M, R.S. Shukla, Biological and clinical aspects of Lanthanide coordination compounds, Bioinorg. Chem. Appl. 2 (2004) 155–192, http://dx.doi.org/10.1155/S1565363304000111.
[14] I. Kostova, Lanthanides as anticancer agents, Curr. Med. Chem. Anticancer Agents 5 (2005) 591–602, http://dx.doi.org/10.2174/156801105774574694.
[15] F. Dimiza, A.N. Papadopoulos, V. Tangoulis, V. Psycharis, C.P. Raptopoulou, D.P. Kessissoglou, G. Psomas, Biological evaluation of non-steroidal

anti-inflammatory drugs-cobalt(ii) complexes, Dalt. Trans. 39 (2010) 4517, http://dx.doi.org/10.1039/b927472c.
[16] M.S. Blois, Antioxidant Determinations by the use of a stable Free Radical, Nature 181 (1958) 1199–1200.
[17] W. Brand-Williams, M.E. Cuvelier, C. Berset, Use of a free radical method to evaluate antioxidant activity, LWT - Food Sci. Technol. 28 (1995) 25–30, http://dx.doi.org/10.1016/S0023-6438(95)80008-5.
[18] P. Molyneux, The use of the stable free radical diphenylpicryl-hydrazyl (DPPH) for estimating antioxidant activity, Songklanakarin J. Sci. Technol. 26 (2004) 211–219, http://dx.doi.org/10.1287/isre.6.2.144.
[19] M.L.S. Negri, J.C. Possamai, T. Nakashima, Atividade antioxidante das folhas de espinheira-santa – Maytenus ilicifolia Mart. ex Reiss., secas em diferentes temperaturas, Braz. J. Pharmacog. 19 (2009) 553–556, http://dx.doi.org/10.1590/S0102-695X2009000400007.
[20] M. Ionashiro, C.A.F. Graner, J. Zuanon Netto, Complexometric titration of lanthanides and yttrium, Eclet. Quim. 8 (1983) 29–32.
[21] T.J. Lane, C.S.C, J.A. Durkin, R.J. Hooper, Infra-red absorption spectra of metal-amino acid complexes—II. An infra-red study of the metal-nitrogen bond in glycine chelates, Spectrochim. Acta 20 (1964) 1013–1019, http://dx.doi.org/10.1016/0371-1951(64)80101-6.
[22] G.B. Deacon, R.J. Philips, Relationships between the carbon-oxygen stretching frequencies of carboxylato complexes and the type of carboxylate coordination, Coord. Chem. Rev. 33 (1980) 227–250.
[23] V. Zelenák, Z. Vargová, K. Gyoryová, Correlation of infrared spectra of zinc(II) carboxylates with their structures, Spectrochim. Acta – Part A: Mol. Biomol. Spectrosc. 66 (2007) 262–272, http://dx.doi.org/10.1016/j.saa.2006.02.050.
[24] J.A. Fernandes, R.A. Ferreira, M. Pillinger, L.D. Carlos, I.S. Gonçalves, P.J.A. Ribeiro-Claro, Spectroscopic studies of europium(III) and gadolinium(III) tris-β-diketonate complexes with diazabutadiene ligands, Eur. J. Inorg. Chem. 19 (2004) 3913–3919, http://dx.doi.org/10.1002/ejic.200400191.
[25] L.D. Carlos, J.A. Fernandes, R.A. Sa Ferreira, O.L. Malta, I.S. Gonçalves, P. Ribeiro-Claro, Emission quantum yield of a europium(III) tris-β-diketonate complex bearing a 1,4-diaza-1,3-butadiene: comparison with theoretical prediction, Chem. Phys. Lett. 413 (2005) 22–24, http://dx.doi.org/10.1016/j.cplett.2005.07.033.
[26] R. Gaur, M. Azizi, J. Gan, P. Hansal, K. Harper, R. Mannan, A. Panchal, K. Patel, M. Patel, N. Patel, J. Rana, A. Rogowska, British Pharmacopoeia 39 (2009) (2009) 418–420, http://dx.doi.org/10.1177/004057368303900411.